RSC Advances

RSCPublishing

Design of $In_xGa_{1-x}As$ buffer layers for epitaxial growth of high-quality $In_{0.3}Ga_{0.7}As$ films on GaAs substrates

Cite this: *RSC Advances*, 2013, **3**, 3973

Pingping Wu,[a] Fangliang Gao,[a] Kelvin H. L. Zhang[b] and Guoqiang Li*[a]

A phase field model is developed to simulate $In_{0.3}Ga_{0.7}As$ thin films grown on an GaAs substrate with different buffer layer structures. Using this newly developed phase field model, an optimal step graded $In_xGa_{1-x}As$ buffer layer structure with four sub-layers of x = 0.09, 0.18, 0.27, and 0.33 is then proposed for epitaxial growth of high-quality $In_{0.3}Ga_{0.7}As$ film on GaAs substrate. The strain distribution analysis by using the phase field model reveals that the compressive strain in this optimal heterostructure is partially balanced by the tensile strain caused by the uppermost two layers of $In_{0.3}Ga_{0.7}As$ grown on top of $In_{0.33}Ga_{0.67}As$, which results in high-quality $In_{0.3}Ga_{0.7}As$ film. The subsequent epitaxial growth of $In_{0.3}Ga_{0.7}As$ films on GaAs substrates demonstrates that the surface RMS roughness and the full width at half maximum of X-ray rocking curve of as-grown $In_{0.3}Ga_{0.7}As$ film with the optimal buffer layer structure are as low as 0.56 nm and 116′′, respectively, indicating very high film quality. These experimental results confirm the high effectiveness of the proposed approach to design buffer layer structure using our newly developed phase field model. This phase field model should be able to extend to hetero-epitaxial growth of other material systems apart from InGaAs.

Received 9th July 2012,
Accepted 2nd January 2013

DOI: 10.1039/c2ra21397d

www.rsc.org/advances

Introduction

Recently, multi-junction solar cells have attracted much interest because of their high efficiency which drives rapid growing market demand with many potential applications. The efficiencies can reach higher than 40% by triple-junction solar cell approaches.[1–4] The theoretical prediction shows that the addition of a 1 eV junction as a bottom junction is effective to increase the triple-junction solar cell efficiency.[5,6] $In_{0.3}Ga_{0.7}As$ can be used for a 1 eV junction,[7] but it has a relatively large lattice misfit strain (~2%) on a GaAs substrate.[8,9] Such a large misfit strain will induce non-ideal epitaxial growth because the alloy layer relaxes by introduction of high dislocation density or the formation of three dimensional islands.[10,11]

In order to minimize the density of threading dislocations caused by the strain relaxation and provide a high quality layer with a new lattice constant for the rest of the sub-cells to be grown on, a very frequently used relaxation technology in solar cells is the compositional step graded buffer layer. The buffer structure introduces graded interfaces for the edge dislocations lying in the interface plane with the Burger's vector in the x–y direction.[12] To relax the misfit strain in the $In_{0.3}Ga_{0.7}As$ thin film on the GaAs substrate, a widely studied compositional buffer layer system is the step graded $In_xGa_{1-x}As$ structures where x gradually increases from 0 (GaAs) to 0.3 ($In_{0.3}Ga_{0.7}As$).[13–16] However, fundamentally understanding the physical mechanism in the buffer layers requires the strain distribution in the step graded multi-layers and its influence on the surface roughness. Thus the optimized structures for buffer layers can be predicted based on theory studies.

The mesoscopic simulations can predict the structures and inner structures of material with strain distribution, which can be directly compared with experimental works. In the last decade, phase field method proved to be a powerful tool to simulate self-assembled quantum dots/thin film structures. Wang *et al.* firstly employed the phase-field model on the surface instability problems.[17] Seol and co-workers studied the shape of the quantum dot structures in Ge/Si systems,[18] Ni *et al.* discussed the morphologies of the heteroepitaxial films with elastic anisotropy,[19] Takaki *et al.* studied the interface energy effect on the shape of the quantum dots.[20] In this work, we have developed a phase field model for epitaxial growth of $In_xGa_{1-x}As$ (x = 0–0.3) films on GaAs. The purpose of this work is to determine an optimal buffer layer structure for $In_{0.3}Ga_{0.7}As$ grown on GaAs based on this newly developed model. The strain distribution and the root-mean-square (RMS) roughness of the thin film surface are studied by the addition of four different artificially designed buffer layer structures, and hence the optimal buffer layer structure has been revealed. We have also grown $In_{0.3}Ga_{0.7}As/In_xGa_{1-x}As$ buffer layer/GaAs heterostructures using these four artificially designed buffer layer structures, which confirm that the optimal buffer layer structure is effective to improve

[a]*State Key Laboratory of Luminescent Materials and Devices, South China University of Technology, Guangdong 510641, China. E-mail: msgli@scut.edu.cn*
[b]*Department of Chemistry, University of Oxford, Oxford, OX1 3QR, UK*

$In_{0.3}Ga_{0.7}As$ film's quality. Obviously, the simulation results help us to better understand the intrinsic mechanism of the strain relaxation by the multi-layered thin film structures and improve the thin film quality of $In_{0.3}Ga_{0.7}As$ grown on GaAs with optimized design of the composition graded buffer layers.

Simulation method

In order to describe the $In_xGa_{1-x}As$ thin film grown on the GaAs(001) substrate, in phase field model, we introduced three conserved order parameters η_1, η_2 and η_3 to describe the volume fractions of gas, thin film and substrate phases respectively. The total volume fraction of the system is fixed,

$$\eta_1 + \eta_2 + \eta_3 = 1 \tag{1}$$

The interface between order parameters η_i and η_j is denoted as γ_{ij}. In the present study, the total free energy is the sum of chemical energy, interface energy and elastic energy

$$F_{\text{tot}} = F_{\text{chem}} + F_{\text{inter}} + F_{\text{elas}} \tag{2}$$

The Landau-type coarse-grained bulk chemical free energy is

$$F_{\text{chcm}} \int -\left[\omega_{12}\eta_1^2\eta_2^2 + \omega_{13}\eta_1^2\eta_3^2 + \omega_{23}\eta_2^2\eta_3^2\right] dv \tag{3}$$

where ω_{12}, ω_{13}, ω_{23} are the heights of the double well potential, and v is the total volume of the system. The interfacial energy between the order parameters in the system can be written as,

$$F_{\text{inter}} = \int -\left[\alpha_{12}^2 \nabla\eta_1 \cdot \nabla\eta_2 + \alpha_{13}^2 \nabla\eta_1 \cdot \nabla\eta_3 + \alpha_{23}^2 \nabla\eta_2 \cdot \nabla\eta_3\right] dv \tag{4}$$

where α_{12}, α_{13}, α_{23} are the gradient energy coefficients. The elastic energy of the thin film at a given strain state is calculated by employing Khachaturyan's microelastic theory,[21]

$$F_{elas} = \frac{1}{2}\int \left[C_{ijkl}\left(\varepsilon_{ij} - \varepsilon_{ij}^0\right)\left(\varepsilon_{kl} - \varepsilon_{kl}^0\right)\right] dv \tag{5}$$

where C_{ijkl} is the second order elastic tensor, the ε_{ij} is the total strain in the microelastic theory, and $\varepsilon_{ij}{}^0$ is the eigenstrain of the material, where

$$\varepsilon_{ij}^0 = \sum_{p=1}^{3} \eta_p \varepsilon_{ij}^{0,\eta_p} \tag{6}$$

For a homogeneous system, the eigenstrain can be written as

$$\sigma_{ij} = C_{ijkl}\left(\varepsilon_{kl} - \varepsilon_{kl}^0\right) = \varepsilon_{ijkl}\left(\varepsilon_{kl} - \sum_{p=1}^{3} \eta_p \varepsilon_{kl}^{0,\eta_p}\right) \tag{7}$$

The mechanical equilibrium condition gives

$$\frac{\partial \sigma_{ij}}{\partial r_j} = C_{ijkl}\left(\frac{\partial \varepsilon_{kl}}{\partial r_j} - \sum_{p=1}^{3} \varepsilon_{kl}^{0,\eta_p} \frac{\partial \eta_p}{\partial r_j}\right) \tag{8}$$

where r is the Cartesian coordinates. Following Khachaturyan, the total strain can be divided in to two parts, the homogeneous part and heterogeneous part, *i.e.*

$$\varepsilon_{ij} = \bar{\varepsilon}_{ij} + \delta\varepsilon_{ij} \tag{9}$$

where the homogeneous strain $\bar{\varepsilon}_{ij}$ is set as the average macrostrain in the system, and the heterogeneous part $\delta\varepsilon_{ij}$ satisfies

$$\int \delta\varepsilon_{ij} dv = 0 \tag{10}$$

According to elastic equilibrium equations, the heterogeneous part can be written as the derivation of the displacement with respect to the coordinates,

$$\delta\varepsilon_{kl} = \frac{1}{2}\left[\frac{\partial u_k}{\partial r_1} + \frac{\partial u_1}{\partial r_k}\right] \tag{11}$$

Substitute (9) and (11) into (8), then we have

$$C_{ijkl}\frac{\partial^2 u_k}{\partial r_j \partial r_1} = \sum_{p=1}^{3} \delta_{ij}^{0,\eta_p} \frac{\partial \eta_p}{\partial r_j} \tag{12}$$

where,

$$\delta_{ij}^{0,\eta_p} = C_{ijkl}\varepsilon_{kl}^{0,\eta_p} \tag{13}$$

Eqn (12) can be solved in the Fourier space, applying the Fourier transforms to both sides of the differential equation

$$v_k = -iG_{ik}\sum_{p=1}^{3} \delta_{ij}^{0,\eta_p} g_i \{\eta_p\}_g \tag{14}$$

where $i^2 = -1$, g is the reciprocal lattice vector in the Fourier space, g_i is the i^{th} component of g, where

$$v_k = \int u_k e^{-ig \cdot r} dv \tag{15}$$

$$\{\eta_p\}_g = \int \eta_p e^{-ig \cdot r} dv \tag{16}$$

$$G_{ik}^{-1} = C_{ijkl} g_j g_l \tag{17}$$

The displacement in the reciprocal space v_k can be solved by eqn (14), and the displacement in real space u_k can be received by reverse Fourier transformation, thus the total strain can be calculated from (9) and (11). Substituting the total strain into (5), we obtained the elastic energy of the system. The final total free energy is calculated as the sum of the elastic energy, chemical energy and the interface energy by

Table 1 Lattice constant, elastic constant, and the misfit strain to GaAs substrate for $In_xGa_{1-x}As$ thin film employed in the simulation

Material	Lattice constant (Å)	C_{11} (10^{11} dyn cm^{-2})	C_{12} (10^{11} dyn cm^{-2})	C_{44} (10^{11} dyn cm^{-2})	Misfit (%)
GaAs	5.6419	11.879	5.376	5.94	0%
InAs	6.0583	8.319	4.526	3.95	7.38%
$In_{0.09}Ga_{0.91}As$	5.67812	11.601	5.30255	5.79023	0.57%
$In_{0.1}Ga_{0.9}As$	5.68354	11.523	5.291	5.741	0.74%
$In_{0.15}Ga_{0.85}As$	5.70436	11.345	5.2485	5.6415	1.11%
$In_{0.18}Ga_{0.82}As$	5.71527	11.256	5.2275	5.5917	1.29%
$In_{0.2}Ga_{0.8}As$	5.72518	11.167	5.206	5.542	1.48%
$In_{0.27}Ga_{0.73}As$	5.74876	11.008	5.14375	5.4225	1.86%
$In_{0.3}Ga_{0.7}As$	5.76682	10.811	5.121	5.343	2.21%
$In_{0.33}Ga_{0.67}As$	5.79386	10.615	5.096	5.215	2.56%

eqn (2). For a conserved system, the temporal evolution of the $In_xGa_{1-x}As$ thin film surface morphology grown on the GaAs substrate is governed by nonlinear Cahn–Hilliard equations.

$$\frac{\partial \eta_p}{\partial t} = \nabla\left[M\nabla\left(\frac{\delta F_{tot}}{\delta \eta_p}\right)\right] \tag{18}$$

where M is the dynamic coefficient, t is time, and the semi-implicit Fourier-spectral method is employed to solve eqn (18).[22]

Results and discussion

In the simulations, the chemical energy parameters were chosen to be $\omega_{12} = \omega_{13} = \omega_{23} = 1.0$, the surface energies and interfacial energy are $\alpha_{12} = \alpha_{13} = 0.5$ N m^{-1}, and $\alpha_{23} = 0.26$ N m^{-1}.[23,24] The lattice constants, mismatch strain, and elastic constants for GaAs, InAs and $In_xGa_{1-x}As$ with various x values are listed in Table 1,[25,26] $256\Delta x_1 \times 64\Delta x_2$ discrete grid points are employed in this work with periodic boundary conditions applied along x_1 axes, where $\Delta x_1 = \Delta x_2 = 1.0$ nm. The initial surface morphology is described by the thin film thickness $h(x)$, which is described by a sinusoidal static plane wave

$$h(x) = h_0\ \beta\sin(kx + \phi) \tag{19}$$

where h_0 is the initial average thin film thickness, β is the amplitude, k is the wave number, and ϕ is the initial phase of the plane wave. In this work, we assume $\beta = 5$ nm and $k = 2\pi/32\Delta x_1$.

Fig. 1a illustrates a classical schematic model of the $In_{0.3}Ga_{0.7}As$ thin film heterogeneous nucleation on the GaAs substrate. The gas, thin film and substrate phases are separated by the interface between any two of them. Different surface morphology can be obtained by changing the initial average thin film thickness h_0 in eqn (19). The typical stable surface morphologies of $In_{0.3}Ga_{0.7}As$ for $h_0 = 5$ nm, 7 nm, 12 nm are shown in Fig. 1b–d, respectively. All the calculations are taken by 1000 time steps with a time step for integration of $\Delta t = 0.1$. At a relatively small average thickness, *i.e.*, $h_0 = 5$ nm, the thin film structure is not stable and evolved to the nanodot structure in order to relax the intrinsic strain, as seen in many previous theoretical and experimental works.[27] With the increase in the average thickness, the layer strain can be relaxed as the elastic energy density is reduced due to the volume of thin film increases and fewer interfaces are introduced. The morphology of the thin film will exhibit a nanohole-like structure (Fig. 1c), and eventually generated a relatively flat thin film at a high average thickness (Fig. 1d).

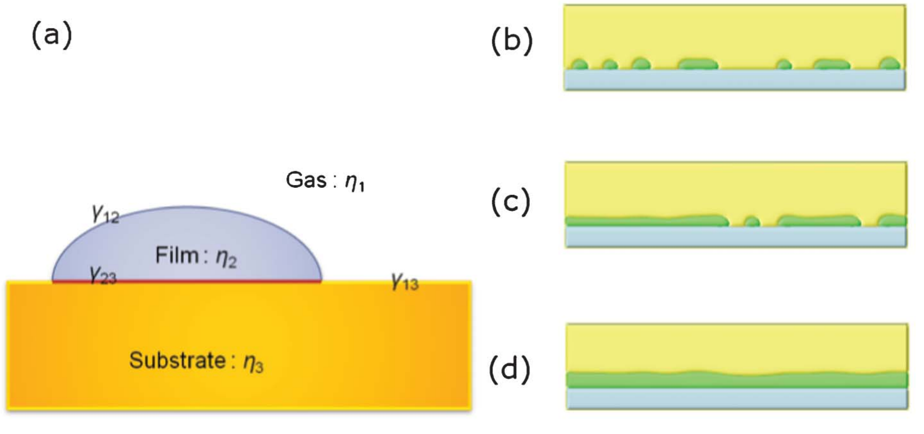

Fig. 1 (a) The schematic of a thin film deposited on the substrate. (b–d) $In_{0.3}Ga_{0.7}As$ thin film grown on GaAs substrate with the h_0 = 5, 7, 12 nm, respectively.

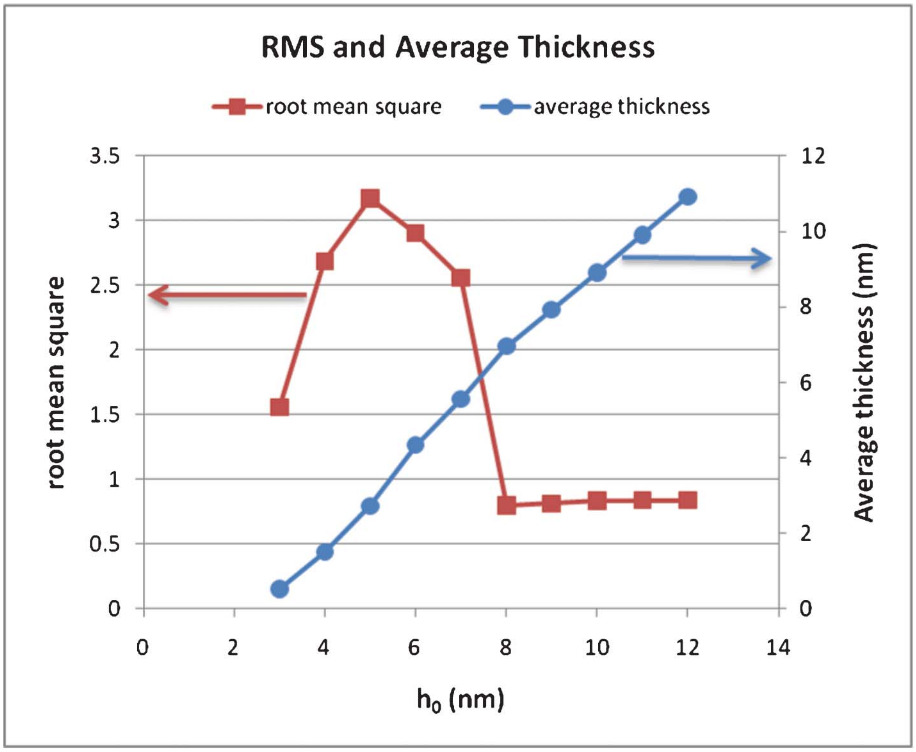

Fig. 2 The root-mean-square roughness and the mean height of the $In_{0.3}Ga_{0.7}As$ nanodot/thin film surface, as a function of initial average film thickness h_0.

The residual strain has a strong influence on the film surface morphology, especially surface roughness. Therefore, we use surface roughness as criterion to evaluate the quality of the "as-grown" films. In order to describe the surface roughness of a solid thin film, the most common statistic used is the root-mean-square (RMS) roughness, which is defined as,[28]

$$RMS = \sqrt{\langle [h(x) - \bar{h}]^2 \rangle} \tag{20}$$

where $\bar{h}$ is the mean height of the thin film surface. In the phase field model, we suggest the distance between the point where $\eta_1 = \eta_2 = 0.5$ and $\eta_2 = \eta_3 = 0.5$ as the height of the surface. The RMS roughness and the mean height of the nanodot/thin film surface for different h_0 are plotted in Fig. 2. With the increase of h_0, we observed an initial increase in the RMS roughness. At this stage, the surface morphologies perform as nanodot structures, with more and more nanodots generated due to the increase of the h_0, which induced the increase of the RMS. When h_0 exceeds 5 nm, the RMS starts to decrease, which is due to the generation of the nanohole structure and the shrinking of all the interfaces. If the h_0 is larger than 8 nm, only a thin film structure was observed. Thus we obtained relatively small RMS for thin films, and we observed minor changes of the RMS for the thin film structures if we continued to increase the h_0. For comparison, it is reasonable that the mean height of the thin film/nanodot structure is linearly proportional to the h_0.

In order to decrease the RMS roughness on the top surface of the $In_{0.3}Ga_{0.7}As$ thin film, a step graded $In_xGa_{1-x}As$ buffer layer is added between the $In_{0.3}Ga_{0.7}As$ thin film layer and GaAs substrate. To obtain optimized buffer structure for $In_{0.3}Ga_{0.7}As$ thin film, four types of different buffer layer systems are suggested in this work. The schematic of the four designed buffer layer structures are shown in Fig. 3. Type I is a single $In_{0.15}Ga_{0.85}As$ buffer layer. In Type II, we used $In_{0.1}Ga_{0.9}As$ and $In_{0.2}Ga_{0.8}As$ bi-layer buffer structure. For Type III, a composition buffer structure of $In_{0.09}Ga_{0.81}As$/$In_{0.18}Ga_{0.82}As$/$In_{0.27}Ga_{0.73}As$ is employed. As for Type IV, its

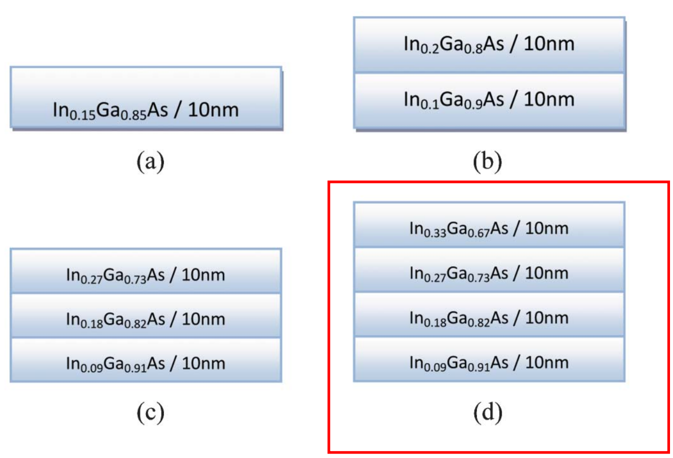

Fig. 3 (a–d) Four types of designed epitaxial buffer layer structures.

buffer structure is based on Type III, with an additional layer with higher composition on the top of Type III buffer stacking structure. For each $In_xGa_{1-x}As$ layer with a certain x value, its thickness is set as 10 nm. We then perform the same procedure as described in Fig. 2, only to find that a further increase in thickness of each individual $In_xGa_{1-x}As$ layer doesn't bring up a smoother surface. In other words, 10 nm thickness of each individual $In_xGa_{1-x}As$ layer is sufficient to release the strain from its bottom layer.

For calculations we used the linear approximation to estimate the buffer layer elastic coefficient and lattice parameter, which are shown in Table 1; the in-plane eigenstrain for the thin film layer is

$$\varepsilon_{\mathrm{ij}}^{0}(r)=\frac{a_{In_xGa_{1-x}As}-a_{sub}}{a_{sub}} \tag{21}$$

where $\varepsilon_{ij}{}^{0}(r)$ is the eigenstrain in the $In_xGa_{1-x}As$ thin film. In our current model, as only three order parameters are introduced, we assume that the $In_{0.3}Ga_{0.7}As$ thin film was fully commensurately grown on the substrate or the top layer of the buffer structures, thus the eigenstrain for no buffer layers and type I–IV buffer layers can be calculated from eqn (21).

Fig. 4(a–e) shows the surface morphology (left) with the strain distribution (right) in the thin film for no buffer layers and type I–IV buffer layers. The simulated surface morphologies show typical sinusoidal wave shapes. We observed a decrease in the magnitude of the strain in the thin film with a division of buffer layers. The calculated eigenstrain and the influence of the designed buffer layer structures induced strain relaxation on the surface RMS roughness are summarized in Table 2. Compared to the $In_{0.3}Ga_{0.7}As$ thin film grown on a GaAs substrate without buffer layers, the RMS roughness for the thin film with a single buffer layer (Type I) obviously decreases from 0.936 nm to 0.662 nm due to the strain relaxation. From the observed simulation results, we can see only a minor difference of RMS roughness between employing

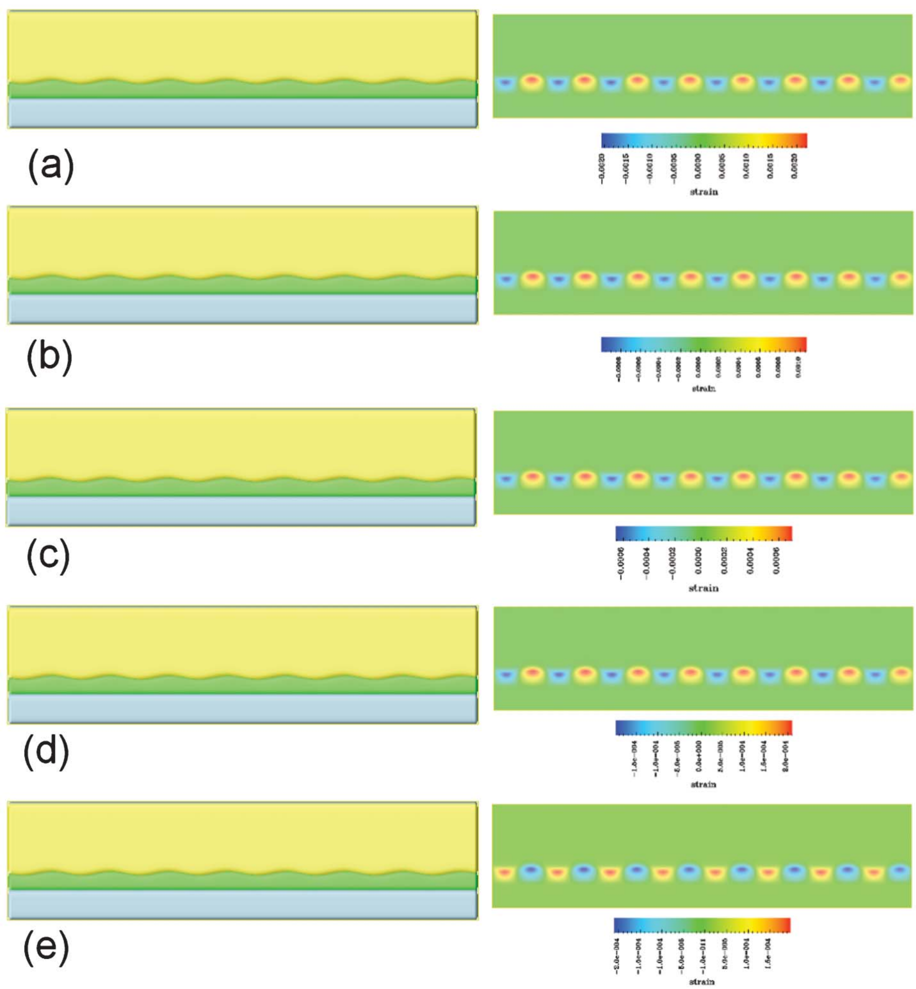

Fig. 4 The surface morphology (left) with the strain distribution (right) for the $In_{0.3}Ga_{0.7}As$ thin film deposited on the GaAs substrate (a) with no buffer layers and (b–e) with four types designed buffer layers in Fig. 3. (a–d) show compressive strain throughout each individual heterostructure. (e) shows the compressive strain is partially balanced by the tensile strain caused by the uppermost two layers of this heterostructure.

Table 2 Results from both phase field simulation and crystal growth for $In_{0.3}Ga_{0.7}As$ films grown on GaAs substrates with no buffer and four types of designed buffer layer structures

	No buffer	Type I	Type II	Type III	Type IV
Eigenstrain calculated from phase field model	0.0221	0.011	0.0073	0.0022	−0.0022
RMS from phase field simulation (nm)	0.936	0.662	0.636	0.511	0.398
RMS from crystal growth (nm)	3.0	2.1	1.8	1.5	0.56
XRC FWHM from crystal growth ($''$)	710	553	327	218	116

Type I (0.662 nm) and Type II (0.636 nm) buffer layer structures. Considering the lattice mismatches between $In_{0.3}Ga_{0.7}As$ and the upper layer of Type I ($In_{0.15}Ga_{0.85}As$, 1.1% mismatch with $In_{0.3}Ga_{0.7}As$) or Type II ($In_{0.2}Ga_{0.8}As$, 0.73% mismatch with $In_{0.3}Ga_{0.7}As$) buffer layer structure, we can claim that a division of the buffer structures have small influence on the surface roughness if the lattice mismatch is still relatively high. However, for Type III buffer layer structure whose upper layer $In_{0.27}Ga_{0.73}As$ has a much smaller lattice mismatch of 0.35% with $In_{0.3}Ga_{0.7}As$, the surface RMS roughness of $In_{0.3}Ga_{0.7}As$ sharply decreases to 0.511 nm. The further reducing of the lattice mismatch shows its effect. A more attractive phenomenon takes place in Type IV. As noticed, for growth of $In_{0.3}Ga_{0.7}As$ film, the upper layer ($In_{0.33}Ga_{0.67}As$) of the Type IV buffer layer structure shares the same lattice mismatch (0.35%) with that ($In_{0.27}Ga_{0.73}As$) of Type III. However, the $In_{0.3}Ga_{0.7}As$ film grown on the Type IV buffer layer structure exhibits apparently higher film quality than that grown on Type III, with a surface RMS roughness of 0.398 nm *vs.* 0.511 nm. This is attributed to the difference in strain distribution when employing the two types, as shown in Fig. 4. When employing Type III for the growth of the $In_{0.3}Ga_{0.7}As$ film on a GaAs substrate, each individual upper film has a larger lattice constant than its lower layer, Table 1. It indicates the whole heterostructure is under compressive strain. On the contrary, if Type IV is employed, when keeping the same small lattice mismatch as Type III, the compressive strain in this heterostructure is partially balanced by the tensile strain caused by the uppermost two layers of $In_{0.3}Ga_{0.7}As$ grown on top of $In_{0.33}Ga_{0.67}As$, which results in a better film quality, here in appearance, and a smoother surface.

Crystal growth

In order to verify the results from our phase field simulation, we have grown $In_{0.3}Ga_{0.7}As/In_xGa_{1-x}As$ buffer layer/GaAs heterostructures with those four artificially designed buffer layer structures in Fig. 3 using molecular beam epitaxy (MBE). GaAs (001) substrates are ultrasonically cleaned in chemicals and deionized water to remove surface contaminations and then dried by 7N nitrogen before being put into the MBE load-lock chamber with pressure 3.2×10^{-7} Torr where the substrates are degassed for about 1.5 h. The substrates are then transferred into the high vacuum MBE growth chamber at a pressure of 2.0×10^{-9} Torr and annealed at 680 °C for 15 min with As molecular beam protection to further remove surface oxidized layers. The growth of $In_xGa_{1-x}As$ films with various x values is subsequently conducted by adjusting the substrate temperature and the ratios among In (7N), Ga (7N) and As (7N) sources. Eventually, four 100 nm thick $In_{0.3}Ga_{0.7}As$ films with those designed buffer layer structures in Fig. 3 are grown, respectively.

The as-grown $In_{0.3}Ga_{0.7}As$ films are characterized by atomic force microscopy (AFM) and X-ray diffraction (XRD) to evaluate surface roughness and crystallinity, respectively. Fig. 5a and b show the results from the as-grown $In_{0.3}Ga_{0.7}As$ film with the buffer structure of Fig. 3d. More detailed results for as-grown $In_{0.3}Ga_{0.7}As$ films with the four different designed buffer layer

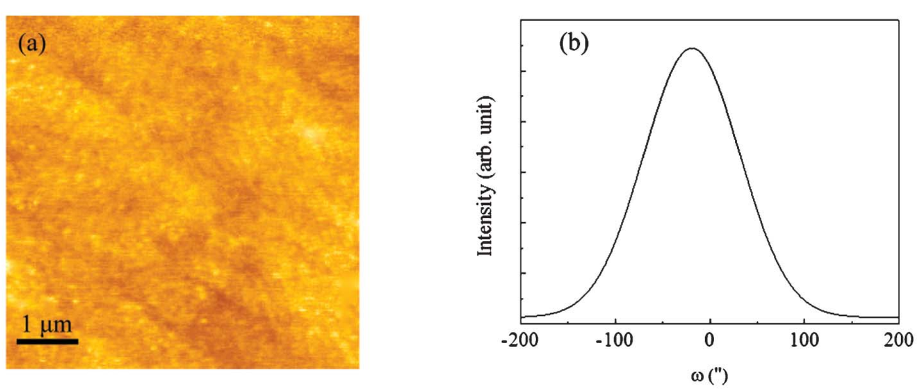

Fig. 5 Characterisation results for $In_{0.3}Ga_{0.7}As$ (001) film epitaxially grown on GaAs (001) substrate using Type IV buffer layer structure. (a) AFM, RMS = 0.56 nm; (b) X-ray rocking curve, FWHM = 116$''$.

structures are listed in Table 2. $In_{0.3}Ga_{0.7}As$ film with Type I buffer layer structure exhibits the highest surface roughness of 3.0 nm, and $In_{0.3}Ga_{0.7}As$ film with type IV buffer layer structure has the lowest surface roughness of 0.56 nm. Although the surface roughness from the as-grown films is larger than that from phase-field simulation, the changing tendencies among these four samples matches well between the crystal growth and the simulation. The crystallinity measurement results from XRD are also consistent with this tendency, with type I buffer layer structure showing the lowest crystallinity, and type IV the best. All these experimental results from crystal growth verify the effectiveness of our proposed approach to design buffer layer structures using phase-field simulation. It should be noted that the surface RMS roughness and the full width at half maximum (FWHM) from X-ray rocking curve (XRC) of the as-grown $In_{0.3}Ga_{0.7}As$ film with Type IV buffer layer structure are as low as 0.56 nm and 116?, respectively, which indicate very high film quality compared with those reported values for $In_{0.3}Ga_{0.7}As$ film.[9–11,29–31] It once again confirms the following two points. First, the proposed phase field simulation is effective to design buffer layer structure for epitaxial growth of $In_{0.3}Ga_{0.7}As$ on GaAs. Second, the proposed optimal buffer layer structure of Type IV as shown in Fig. 3d is efficient to obtain a high quality $In_{0.3}Ga_{0.7}As$ film on GaAs.

However, one can still observe some discrepancies between the model and experimental data. The first observation is that there are distinct differences in the magnitude of the RMS roughness between the simulation results and the experimental works, Table 2. The simulation results predict a relatively small surface roughness (<1.0), however, the experimental RMS roughness varies from 0.5–3.0. Please note that some natural factors are not included in our current model. Firstly, the model only contains three order parameters, which introduce three interfaces between the gas, the thin film, and the substrate. When a buffer layer is inserted or a division of buffer structure is employed, the $In_{0.3}Ga_{0.7}As$ thin film is assumed to fully commensurately grow on the top layer of the buffer structures. This leads to the varying degrees of eigenstrain in the thin film layer, but the interfaces in the buffer layers are not addressed at the moment. Actually, the interfaces in the buffer structures can reduce the surface roughness by shape changing and interface motion due to diffusion. Secondly, our model doesn't include any crystal defects. The effects of defects on the morphology instabilities can induce an increase in the RMS roughness. To introduce defects into the model will be the focus of our future work.

Based on the theory, the magnitudes of eigenstrain in the thin films of Type III and Type IV are the same, which induces similar surface RMS roughness in simulation. However, in experimental works, Type IV supplied a much smoother representation of the surface compared to Type III. When employing Type III for growth of $In_{0.3}Ga_{0.7}As$ film on GaAs substrate, each individual upper film has a larger lattice constant than its lower layer, Table 1. It indicates that the whole heterostructure is of compressive strain. On the contrary, if Type IV is employed, when keeping the same small lattice mismatch as Type III, the compressive strain in this heterostructure is partially balanced by the tensile strain caused by the uppermost two layers of $In_{0.3}Ga_{0.7}As$ grown on top of $In_{0.33}Ga_{0.67}As$, which results in a better film quality; here in appearance, a smoother surface. In simulation, on the contrary, the phase field model assumes that the $In_{0.3}Ga_{0.7}As$ thin film grown on the top layer of the buffer structures is fully commensurate. Therefore, it is not surprising that similar RMS roughness was received for Type III and Type IV in simulation.

Conclusion

A phase field model is developed to simulate the $In_{0.3}Ga_{0.7}As$ thin film grown on the GaAs substrate with different buffer layer structures. The surface morphology, RMS roughness and the mean height of nanodot/thin film structures are studied in detail. The mean height of the thin film is linear to the initial average thickness h_0 in the model. It is shown that the RMS roughness increases at a relatively small h_0, then the surface roughness decreases with a further increase in the average thickness and eventually kept constant and a flat thin film generated.

To obtain a high quality $In_{0.3}Ga_{0.7}As$ epitaxial film on a GaAs substrate, four types of step graded $In_xGa_{1-x}As$ buffer layer structures are designed. Using the newly developed phase field model, an optimal step graded $In_xGa_{1-x}As$ buffer layer with four sub-layers of x = 0.09, 0.18, 0.27, and 0.33 is then found. The strain distribution analysis using the phase field model reveals that the compressive strain in this optimal heterostructure is partially balanced by the tensile strain caused by the uppermost two layers of $In_{0.3}Ga_{0.7}As$ grown on top of $In_{0.33}Ga_{0.67}As$, which leads to a high quality $In_{0.3}Ga_{0.7}As$ film.

The subsequent crystal growth of $In_{0.3}Ga_{0.7}As$ films on GaAs substrates using these four designed buffer layer structures reveals that both the surface roughness and the crystallinity from the as-grown $In_{0.3}Ga_{0.7}As$ films share the same tendency with our phase-field simulation. Particularly, the surface RMS roughness and the XRC FWHM of as-grown $In_{0.3}Ga_{0.7}As$ film with the optimal buffer layer structure are as low as 0.56 nm and 116?, respectively, indicating very high film quality. These experimental results demonstrate the high effectiveness of our proposed approach to design a buffer layer structure using our newly developed phase field model.

In the procedures of simulation, some factors such as defects in films are ignored. Meanwhile, there might be also factors that we think unimportant that have not been taken into account. Accordingly, the model in this work is not perfect when compared with the actual epitaxial growth. But nevertheless, the simulation represented in this work helps us better understand the intrinsic mechanism of the strain relaxation by the multi-layered thin film structures and improve the thin film quality of $In_{0.3}Ga_{0.7}As$ grown on GaAs with optimized design of the composition graded buffer layers.

This phase field model should be able to extend to hetero-epitaxial growth of other material systems apart from InGaAs.

Acknowledgements

This work is supported by National Key Basic Research Project of China (973 Project), National Science Foundation of China (Contract No. 51002052), and Key Project in Science and Technology of Guangdong Province (Contract Nos. 2011A080801018, and 2011A081301014).

References

1 J. Lee, Z. Wang, Y. Hirono, E. Kim, N. Kim, S. Park, C. Wang and G. J. Salamo, *CrystEngComm*, 2010, **12**, 3404.
2 M. Heigoldt, J. Arbiol, D. Spirkoska, J. M. Rebled, S. Conesa-Boj, G. Abstreiter, F. Peiró, J. R. Morante and A. F. i Morral, *J. Mater. Chem.*, 2009, **19**, 840.
3 M. Wiemer, V. Sabnis and H. Yuen, *Proc. SPIE–Int. Soc. Opt. Eng.*, 2011, **8108**, 810804.
4 A. Luque, *J. Appl. Phys.*, 2011, **110**, 031301.
5 S. R. Kurtz, D. Myers and J. M. Olson, *26th IEEE Photovoltaic Specialists Conference*, 1997, 875.
6 D. J. Friedman, *et al.*, 0.7 eV GaInAs Junction for a GaInP/GaAs/GaInAs(1 eV)/GaInAs(0.7 eV) Four-Junction Solar Cell, *4th World Conf. on Photovoltaic Energy Conversion*, 2006, 598.
7 J. F. Geisz, S. R. Kurtz, M. W. Wanlass, J. S. Ward, A. Duda, D. J. Friedman, J. M. Olson, W. E. McMahon, T. E. Moriarty, J. T. Kiehl, M. J. Romero, A. G. Norman and K. M. Jone, *33rd IEEE Photovoltaic Specialists Conference San Diego*, California, May 2008, 11–16.
8 F. Camacho-Alanis, L. Wu, G. Zangari and N. Swami, *J. Mater. Chem.*, 2008, **18**, 5459.
9 M. R. Pillai, Seong-Soo Kim, S. T. Ho and S. A. Barnett, *J. Vac. Sci. Technol., B*, 2000, **18**(3), 1232.
10 J. W. Matthews and A. E. Blakeslee, *J. Cryst. Growth*, 1976, **32**, 265.
11 J. M. Millunchick and S. A. Barnett, *Appl. Phys. Lett.*, 1994, **65**, 1136.
12 J. H. Lee, Z. M. Wang, M. E. Ware, K. C. Wijesundara, M. Garrido, E. A. Stinaff and G. J. Salamo, *Cryst. Growth Des.*, 2008, **8**, 1947.
13 J. C. P. Chang, Jianhui Chen, J. M. Fernandez, H. H. Wieder and K. L. Kavanagh, *Appl. Phys. Lett.*, 1992, **60**, 1129.
14 J. C. P. Chang, T. P. Chin, C. W. Tu and K. L. Kavanagh, *Appl. Phys. Lett.*, 1993, **63**, 500.
15 T. B. Mayank, C. Leitz and E. A. Fitzgerald, *Appl. Phys. Lett.*, 1998, **72**, 1608.
16 F. Romanato, E. Napolitani, A. Carnera, A. V. Drigo, L. Lazzarini, G. Salviati, C. Ferrari, A. Bosacchi and S. Franchi, *J. Appl. Phys.*, 1999, **86**, 4748.
17 Y. U. Wang, Y. M. Jin and A. G. Khachaturyan, *Acta Mater.*, 2004, **52**, 81.
18 D. J. Seol, S. Y. Hu, Z. K. Liu, L. Q. Chen, S. G. Kim and K. H. Oh, *J. Appl. Phys.*, 2005, **98**, 044910.
19 Y. Ni, L. H. H and A. K. Soh, *J. Cryst. Growth*, 2005, **284**, 281.
20 T. Takaki, T. Hirouchi and Y. Tomita, *J. Cryst. Growth*, 2008, **310**, 2248.
21 A. G. Khachaturyan, *Theory of Structural Transformations in Solids*, Wiley, New York, 1983.
22 L. Q. Chen and J. Shen, *Comput. Phys. Commun.*, 1998, 108.
23 I. V. Kurilo and S. K. Guba, *Inorg. Mater.*, 2011, **47**, 819.
24 T. Anan, K. Nishi and Sigeo Sugou, *Appl. Phys. Lett.*, 1992, **60**, 3159.
25 S. L. Chuang, *Physics of Optoelectronics Devices*, Wiley, New York, 1995.
26 S. O. Mariager, S. L. Lauridsen, A. Dohn, N. Bovet, C. B. Sørensen, C. M. Schleputz, P. R. Willmott and R. Feidenhans'l, *J. Appl. Crystallogr.*, 2009, **42**, 369.
27 P. Sutter and M. G. Lagally, *Phys. Rev. Lett.*, 2000, **84**, 4637.
28 M. Pelliccione and T. M. Lu, *Evolution of Thin Film Morphology Modeling and Simulations*, Springer, 2007.
29 X. Yang, M. J. Jurkovic, J. B. Heroux and W. I. Wang, *Appl. Phys. Lett.*, 1999, **75**, 178.
30 J. C. Shin, K. H. Kim, K. J. Yu, H. Hu, L. Yin, C. Z. Ning, J. A. Rogers, J. M. Zuo and Xiuling Li, *Nano Lett.*, 2011, **11**, 4831.
31 H. Q. Nguyen, E. Y. Chang, H. W. Yu, H. D. Trinh, C. F. Dee, Y. Y. Wong, C. H. Hsu, B. T. Tran and C. C. Chung, *Appl. Phys. Express*, 2012, **5**, 055503.